Arabian Journal for Science and Engineering (2023) 48:13283–13302
https://doi.org/10.1007/s13369-023-07660-9

RESEARCH ARTICLE-CIVIL ENGINEERING

Effects of Building Height and Seismic Load on the Optimal Performance of Base Isolation System

Aloys Dushimimana[1] · Cyrille Dushimimana[2] · Leopold Mbereyaho[3] · Aude Amandine Niyonsenga[4]

Received: 8 May 2022 / Accepted: 25 January 2023 / Published online: 17 March 2023
© The Author(s) 2023

Abstract
Seismic isolation has been widely accepted as one of the techniques that can be used to protect structures during earthquake ground motions. However, some challenges still exist such as the optimal control of excessive isolator shear strains imposed by some ground motions. The main purpose of this study was to assess the effects of building height variation and earthquake ground motion type on the optimal performance of the seismic isolation using lead core rubber bearing (LCRB). Nonlinear time history analysis for building models of various storeys isolated by LCRB and exposed to different real earthquakes was performed. To achieve this, the equations governing the motion of the isolated three different building models were presented, and an approach for solving the equations while taking into consideration of the optimized mechanical properties of the LCRB was developed. The LCRB performance was measured in terms of elastomer shear strains, derived after an optimal criterion leading to reliable substructure and superstructure responses was reached. The results showed that the combined effects of the earthquake type and building height significantly affect the substructure responses (maximum isolator displacement, energy dissipation capacity, maximum isolator force) and the superstructure responses (storey shear forces, storey drifts, floor displacements, and floor accelerations), which in some cases lead to a need for adding a fluid damper. In this regard, an attempt to couple the LCRB with nonlinear fluid viscous damper was made, and the performance of the hybrid was assessed. It was generally found that the hybrid can positively improve the substructure responses, thereby reducing the unwanted large elastomer shear strains without adversely affecting the superstructure responses.

Keywords Seismic isolation · Elastomer shear strain · Energy dissipation · Near-fault · Far-fault · Fluid viscous damper

Abbreviations

LCRB	Lead core rubber bearing
FVD	Fluid viscous damper
MID	Maximum isolator displacement
MIF	Maximum isolator force
EDC	Energy dissipation capacity
MPs	Isolator mechanical properties
ASCE	American Society of Civil Engineers
PGV	Peak ground velocity
PGA	Peak ground acceleration
MDOF	Multi-degree-of-freedom system
FF	Far-fault earthquake
NF	Near-fault earthquake
TSS	Total shear strain

List of Symbols

$M_{n\times n}$	Mass matrix for a structure with n floors
$K_{n\times n}$	Stiffness matrix for a structure with n floors
$C_{n\times n}$	Damping matrix for a structure with n floors
$U_{n\times 1}$	Vector of displacements for a structure with n floors
$\dot{U}_{n\times 1}$	Vector of velocities for a structure with n floors
$\ddot{U}_{n\times 1}$	Vector of accelerations for a structure with n floors

✉ Aloys Dushimimana
aloysdushimimana@yahoo.fr

1 Department of Civil Engineering, ISISE/IB-S, University of Minho, Guimarães, Portugal

2 Institute for Basic Science, Technology and Innovation, Pan African University, Nairobi, Kenya

3 Department of Civil, Environmental and Geomatic Engineering, College of Science and Technology, University of Rwanda, Kigali, Rwanda

4 Department of Architecture and Civil Engineering, Shaoxing University, Shaoxing, China

U^*	Vector of modal displacements relative to the base
$\dot{U}^*$	Vector of modal velocities relative to the base
$\ddot{U}^*$	Vector of modal accelerations relative to the base
$\ddot{U}_g$	Vector of earthquake ground accelerations
U_b	Vector of base displacements
$\dot{U}_b$	Vector of base velocities
$\ddot{U}_b$	Vector of base accelerations
$\ddot{U}_{b1\times1}$	Unity vector of base acceleration (the index 1×1 indicates a one-by-one vector, and the same is applicable to where else is found throughout the text)
$R_{n\times1}$	Influence matrix vector for a structure with n floors
G	Shear modulus of the elastomer
m	Number of eigenvectors retained in the analysis
ξ_i	Modal damping ratio
ω_i	Natural frequency of fixed base structure in the mode i
C_b	Resultant damping matrix of viscous isolation element
K_b	Resultant stiffness matrix of elastic isolation elements
α	Ratio of post-yield to pre-yield stiffness for the isolation element
Z	Component of Wen's nonlinear model
u_y	Yield displacement of the isolation element
β, A and τ	Dimensionless parameters defined based on laboratory experiments
η	A constant which controls the transition from elastic to plastic behaviour of the Wen's nonlinear model
ξ_b	Bearing damping ratio
T_b	Bearing natural period
g	Acceleration of gravity ($g = 9.81$)
M_{sup}	Total mass of the superstructure
W	Total weight of structure
Kn	Superstructure stiffness at nth floor
Cn	Superstructure damping at nth floor
m_n	Superstructure mass at nth floor
Q_d	Characteristic strength ratio
F_o	Normalized yield strength
f	A vector containing forces mobilized in the nonlinear elements of the isolation system
T_q	Total thickness of the elastomer active during shear occurrence
K_d	Post-yield stiffness of the isolation element
K_e	Elastic stiffness of the isolation element
K_{eff}	Effective stiffness of the isolation element
K_y	Yield stiffness of the isolation element
ϕ	Modal matrix of fixed base superstructure normalized with respect to mass
f_y	Yield force for the isolation element
ε_{qE}	Shear strains due to earthquake-imposed horizontal displacement
M_b	Diagonal mass matrix of rigid base
$\ddot{U}_{\text{bmax}}$	Maximum base floor acceleration
U_{tmax}	Maximum top floor displacement
d_{bd}	Earthquake-imposed design displacement

1 Introduction

Seismic isolation is a technique that is aimed to decouple a structure from ground shaking using isolator devices. The use of lead core rubber bearing (LCRB) for seismic isolation of structures has been widely accepted as one of the existing techniques that can reduce earthquake energy, thereby allowing the structure to experience less shear forces upon occurrence of the earthquake. LCRB is capable of reducing the structure responses such as isolator displacement [1], base [2] and superstructure [3] accelerations, storey shear forces and drifts [3], and presents reliable hysteretic behaviour in terms of maximum isolator displacement (MID), maximum isolator force (MIF) and energy dissipation capacity (EDC) [1, 2, 4, 5]. When performing a numerical study [6], relative displacement and absolute acceleration were found reduced by 5.5 times and 8.5 times, respectively, as compared to the responses from fixed base structure. Furthermore, when using a nonlinear analytical model to predict the behaviour of the base isolated University of Southern California hospital building [7], nearly 50% of acceleration reduction, peak floor drifts less than 30% of the ASCE code specifications, and yielding of the bearing at the dissipation energy of 20% were observed. With such reliable and promising responses, the application of LCRB device has been extensively considered and adopted. In fact, a good performance of some seismically isolated buildings after different severe earthquakes was reported [8]. For example, it was reported that the Foothill communities' law and Justice Center (FCLJC), built in 1985 and isolated by 98 LCRBs, successfully resisted Northridge earthquake with a magnitude of 8.3 [8]. Another example is the Western Japan postal Center (located in Sanda city), built in 1991 and isolated by 126 LCRBs, which resisted the Kobe Earthquake with a magnitude of 8.18 [8]. However, strong ground motions can cause variation of stresses and shear strains in the elastomer of the bearing, which may consequently lead to undesired performance of the bearing in some cases, like when earthquake beyond the LCRB capacity occurs. In this regard, it has been revealed that the bearing might exhibit instabilities such as buckling, local tensile cracks and even rupture of elastomer (in extreme cases) when subjected to large tensile stresses, the latter being increased with increase in shear strains [9–12]. Also, existing studies

show that the bearing performance can be affected by temperature variation in the lead core as high temperature will lead to yield stress degradation, thereby reducing the bearing characteristic strength [13], and will increase elastomer shear strains due to a decrease in the stiffness and strength of the isolators [8]. Moreover, ageing and environmental effects can change the mechanical properties of the bearing. As example, it was found that the horizontal stiffness can increase or decrease with time depending on the level of the elastomer shear strains [14]. Besides, referring to a durability study conducted on the LCRB for up to 15 years, the compression and shear stiffness can increase with time [15]; besides, ageing factors to account for the variation of the bearing mechanical properties are provided in AASHTO [16].

A numerical investigation on mechanical properties of LCRB when exposed to extreme loading [13] showed that under extended shaking, elastomer shear strains can be large and may exceed 300% in regions highly prone to earthquake hazards. After performing experimental test on a full-scale LCRB and developing a numerical model to predict the response observed during the experiment, it was shown that above 100% shear strains the MID exceeds the height of the rubber and hence hardening phenomenon occurs [17]. In addition, when conducting a numerical study on the response of LCRB exposed to variable axial loads, larger shear strains of up to 125% were found to result in much higher tensile stresses than the recommended values [10], and up to 600% were reported in another numerical study conducted for earthquakes with low peak PGA/PGV [9]. Furthermore, it was reported that the mechanical properties of the bearing will degrade because of substantial energy dissipation resulting from large displacements of the bearing [9] and high-level displacements due to near-fault (NF) earthquake will cause instability in the isolation system, which makes the existing reports related to the performance of LCRB when exposed to NF motions less desirable [18]. Besides, a report showed that earthquakes with high intensity can cause the bearing to experience shear strains exceeding 400%, as a result of large displacements and unstable movements [19]. In addition, in a numerical study conducted on the performance of steel-laminated rubber bearing subjected to both axial loads and strains, it was found that tensile stresses greater than 2 MPa developed when the bearing was exposed to tensile displacements that resulted from a combination of axial displacements of 59 mm, shear strains of 210%, and rotation of 0.0206 radians [11]. It was, furthermore, observed that top and bottom steel shims rotated by 13.8° and 5° when time histories of 0.25 and 0.5 g were imposed, respectively. Such rotations of steel shims could cause degradation of elastomer and plasticity of the shims, and hence leading to failure of the bearing. An experimental study showed that LCRB will fail at 2 MPa tension with only 175% of shear deformation [20]. After performing tensile tests on the bearing and developing theoretical formulations, it was also found that the bearing exhibits nonlinear behaviour for tensile stresses larger than 2 MPa and tensile stiffness of approximately 1/7 of the compressive stiffness, based on tangent stiffness measured from origin [21]. An experimental study [12] showed that the effect of lateral displacement on vertical stiffness of the bearing will become significant only after the lateral shear strain of the bearing exceeds 100%. From the above findings, many authors agree on the fact that tensile stresses larger than 2 MPa are harmful to the LCRB's performance. In fact, with regard to the existing code provisions, BS EN 15129 [22] and EN 1337-3 [23] recommend that the development of tensile stresses within the elastomeric bearings should not exceed $2G$, where G is the shear modulus of elastomer (its value ranging between 0.55 and 1.2 MPa). This means that the allowed tensile stresses in the above codes range between 1.1 and 2.4 MPa. The aseismic design code of China limits the tensile stresses developed in the elastomeric bearing to 1 MPa [21]. However, recommendations from the above provisions are scattered, which indicates that the effects of tensile stresses on the performance of the bearings are not yet fully understood, and therefore more related studies can provide a significant contribution. Tensile stresses exceeding 5 MPa were observed to occur within elastomer when the bearing was subjected to shearing strains larger than 125% [10, 11]. This reveals that large shear strains in the elastomer should be prevented by setting optimal bearing performance criteria that considers the maximum value of the tensile stresses. It is, therefore, of paramount importance to conduct studies on the control of excessive shear strains in the elastomer. This study aims at determining and analysing the elastomer shear strains for different building heights exposed to different types of seismic loads. The shear strains were derived from the obtained promising substructure and superstructure responses. To reduce large shear strains resulting from strong motions, the present study, furthermore, attempted to couple LCRB with nonlinear fluid viscous damper (FVD).

2 Research Significance

Looking at the existing literature, there are many studies on the investigation of the bearing strains, and the examination of the behaviour of the LCRB under axial or a dynamic load; however, a few studies exist on the state when the bearing is used to isolate a multistoried building under a seismic load. Particularly, there are little or no studies that address the combined effects of the type of the seismic load and the building height on the important bearing responses (e.g., MID, MIF, EDC) and the superstructure responses as well (e.g., floor accelerations and displacements, storey drifts and shear forces). In fact, even the studies that consider isolated

multistoried buildings partially examine the substructure and superstructure responses. For example, a main investigation was only performed on the bearing displacement and top floor accelerations by [24], on the bearing responses such as EDC and MID by [25], and on the superstructure responses by [6]. However, information on both the bearing and superstructure responses should be provided as they depend on each other. Furthermore, while many studies exist on the optimization of the bearing mechanical properties [18, 26, 27], there are a few or no studies that develop the optimization considering the bearing shear strains meanwhile incorporating the accuracy, stability, and the time instants conditions. Elastomer shear strains determined incorporating these three conditions depend not only on the responses of the bearing but also on the responses of the superstructure and hence can be regarded as a primary design objective, as they can indicate the overall behaviour of the seismic isolation system. In this context, the present study contributes firstly to presenting a simple strategy for solving the involved equations governing the motion of a building isolated by LCRB. Secondly, the equations are adopted in developing a new optimization process incorporating the mentioned three conditions (also described in Sect. 3.4) used to obtain the optimal mechanical properties of the LCRB, from which the shear strains in the elastomer of the bearing are determined. And thirdly, the study contributes towards assessing the effects of building height variation and earthquake type on the seismic isolation performance, mainly considering the effects on both substructure and superstructure responses. Besides, the effectiveness of coupling LCRB with nonlinear FVD is also assessed.

3 Methods

A detailed description of equations governing a dynamic motion of a structure fixed or isolated at its base, the investigated structural building models, and the strategy for assuring the optimal performance of the isolation system, are provided in this section. The existing equations were used to study the behaviour of a 5-, 10-, and 15-storey building models to investigate the variation of shear strain levels in the elastomer due to building height and seismic load variations. Authors classified the investigated building models as low-rise (5-storey), middle-rise (10-storey), and high-rise (15-storey) structures, which is quite similar to the categorization as per Code for Design of Civil Building [28]. This helped in examining the effects of building heights in the above three categories on the behaviour of the isolation system.

3.1 Assumptions, Scope, and Limitations

In this study, the assumptions, scope, and limitations made are defined as follows.

(i) The present study is pertinent to buildings with symmetric layout. Furthermore, similarity in the stiffness variations of the isolators is assumed to minimize torsional effects. Also, the superstructure behaviour is assumed linear elastic as the isolator is expected to substantially reduce the structural response.
(ii) The horizontal component of the earthquake ground acceleration is applied to the building models; hence the effect of the vertical component is beyond the scope of the present study, this implies that the unidirectional structure motion is assumed with negligible torsion or compression effects.
(iii) The superstructure masses are assumed lumped and concentrated on each floor, the floors and ground are assumed rigid with massless column (see Fig. 1e, f) to ensure rigid body motion; hence, the mass, stiffness, and damping matrices are diagonal.

3.2 Governing Equations

The governing equations for a dynamic motion of building fixed at its base and excited by a seismic load from an earthquake ground motion can be written as:

$$M_{n\times n}\ddot{U}_{n\times 1} + C_{n\times n}\dot{U}_{n\times 1} + K_{n\times n}U_{n\times 1} = -M_{n\times n}R_{n\times 1}\{\ddot{U}_g\} \tag{1}$$

where n is the number of floors, $M_{n\times n}$ is the mass matrix, $K_{n\times n}$ is the stiffness matrix, $C_{n\times n}$ is the damping matrix, $\ddot{U}_g$ is a vector of ground acceleration, $R_{n\times 1}$ is an influence coefficient matrix to imply the pseudo-elastic deformation of the respective floor under a unit deformation of the ground [26], and $U_{n\times 1}$, $\dot{U}_{n\times 1}$ $\ddot{U}_{n\times 1}$ are vectors of displacement, velocity, and accelerations of the structure relative to the base, respectively. For a unidirectional dynamic motion of a structure isolated at its base level, the governing differential equation is formulated below as proposed and adopted in 3D-BASIS Software by [29]:

$$\begin{aligned}
&\begin{pmatrix} [I] & \left[\emptyset^T M R\right] \\ \left[R^T M \emptyset\right] & \left[R^T M R + M_b\right] \end{pmatrix}_{(m+1)(m+1)} \begin{Bmatrix} \ddot{U}^* \\ \ddot{U}_b \end{Bmatrix}_{(m+1)\times 1} \\
&+ \begin{pmatrix} \left[2\xi_i \omega_i\right] & 0 \\ 0 & [C_b] \end{pmatrix}_{(m+1)(m+1)} \begin{Bmatrix} \dot{U}^* \\ \dot{U}_b \end{Bmatrix}_{(m+1)\times 1} \\
&+ \begin{pmatrix} \left[\omega_i^2\right] & 0 \\ 0 & [K_b] \end{pmatrix}_{(m+1)(m+1)} \begin{Bmatrix} U^* \\ U_b \end{Bmatrix}_{(m+1)\times 1} + \begin{Bmatrix} 0 \\ f \end{Bmatrix}_{(m+1)\times 1} \\
&= -\begin{bmatrix} \emptyset^T M R \\ R^T M R + M_b \end{bmatrix}_{(m+1)\times 1} \ddot{U}_{g1\times 1}
\end{aligned} \tag{2}$$

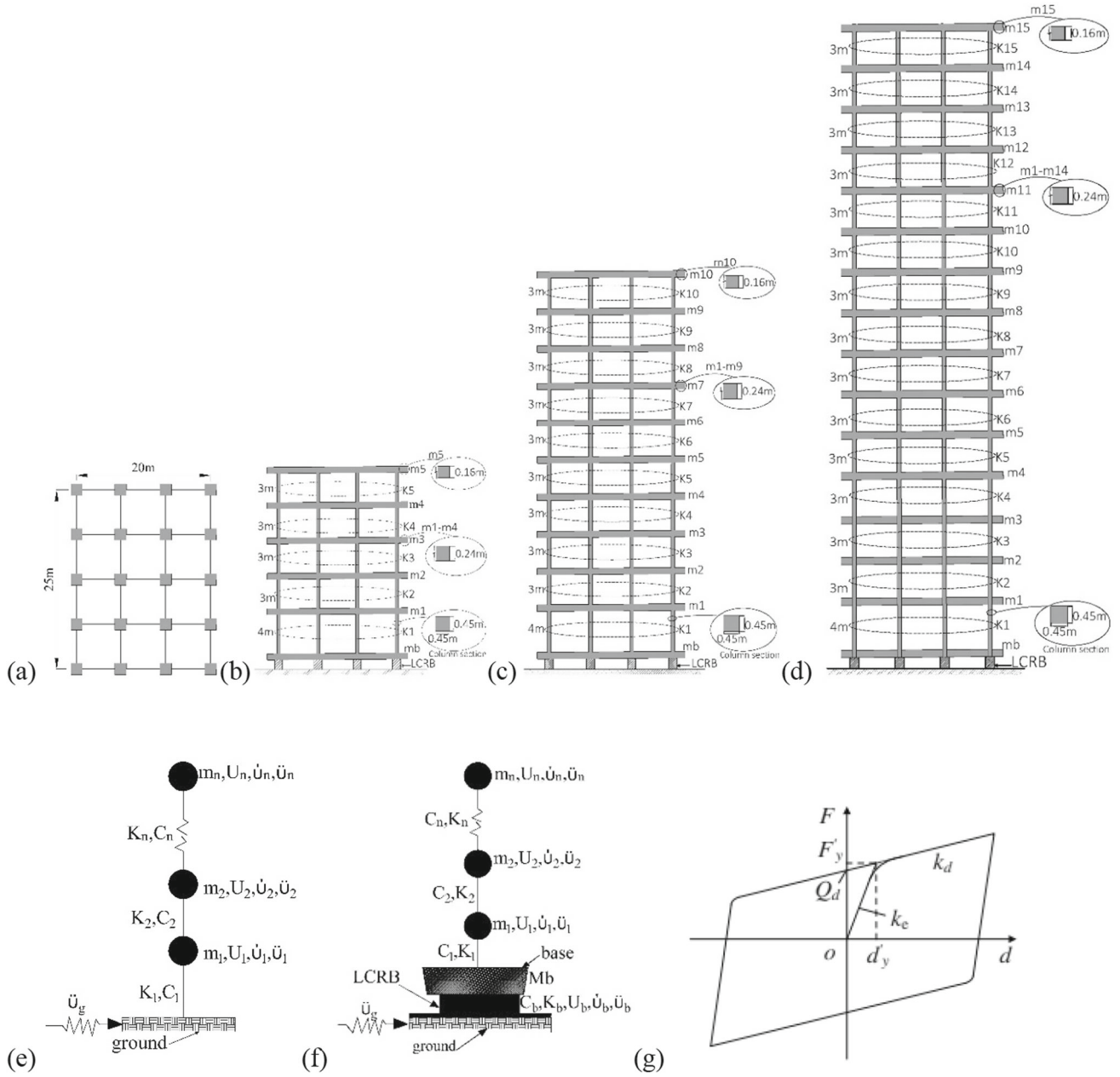


Fig. 1 Structural model: floor plan (**a**), elevation plan for 5 (**b**)-, 10 (**c**)-, and 15 (**d**)-storey building models; the idealized MDOF structure: with fixed base (**e**) and with isolation by LCRB (**f**), and LCRB idealized force displacement (**g**)

where ϕ is the modal matrix of fixed base structure normalized with respect to mass, U^*, $\dot{U}^*$, $\ddot{U}^*$are modal displacement, velocity and acceleration vectors relative to the base, respectively; m is the number of eigenvectors retained in the analysis, ξ_i is a modal damping ratio and ω_i is a natural frequency of fixed base structure in the mode i.M_b is a diagonal mass matrix of rigid base, C_b is a resultant damping matrix of viscous isolation element,K_b is a resultant stiffness matrix of elastic isolation elements,U_b, $\dot{U}_b$, $\ddot{U}_b$ are vectors of base displacement, velocity and accelerations, respectively;f is a vector containing forces mobilized in the nonlinear elements of the isolation system. Expanding Eq. (2) and employing a modal reduction for simplification at n th superstructure floor, these expressions can be obtained:$U_{n\times1} = \phi_{n\times m}U^*_{m\times1}$,$C_{n\times n} = 2\xi_i\omega_i M_{n\times n}$;$K_{n\times n} = {\omega_i}^2 M_{n\times n}$. In this case, Eq. (2) can be rewritten in a separate form where the unidirectional superstructure motion is expressed as [29]:

$$M_{n\times n}\ddot{U}_{n\times1} + C_{n\times n}\dot{U}_{n\times1} + K_{n\times n}U_{n\times1} = -M_{n\times n}R_{n\times1}\left\{\ddot{U}_g + \ddot{U}_b\right\} \quad (3)$$

and the unidirectional substructure (base) motion is expressed as [29]:

$$R_{1\times n}^{T} M_{n\times n}\left\{\left\{\ddot{U}\right\}_{n\times 1} + R_{n\times 1}\left\{\ddot{U}_b + \ddot{U}_g\right\}_{1\times 1}\right\} + M_{b1\times 1}\left\{\ddot{U}_b + \ddot{U}_g\right\}_{1\times 1} + C_{b1\times 1}\left\{\dot{U}_b\right\}_{1\times 1} + K_{b1\times 1}\{U_b\}_{1\times 1} + \{f\}_{1\times 1} = 0 \tag{4}$$

3.3 Solution Method

In this work, a new approach for solving Eqs. (3) and (4) while incorporating optimized mechanical properties (obtained after reaching the defined optimal criterion) of the LCRB is developed. The equation for calculation of the vector f in Eq. (4) is highly stiff nonlinear, due to inclusion of Eq. (16) which is a stiff system considered difficult to solve [30], hence leading to difficulties in finding the appropriate solutions for the governing equations. A few studies, e.g. [26], describe the solution methods particularly by introducing techniques used when determining the vector f; hence, one of the contributions of this work is to further increase the number of literatures with detailed solution methods. To begin with, Eqs. (3) and (4) are first written in a simpler form, and new formulations that can easily be solved using available methods for solving stiff differential equations are deduced as follows.

(a) From Eq. (3), $\ddot{U}_{n\times 1}$ can be determined as:

$$\ddot{U}_{n\times 1} = -R_{n\times 1}\left(\ddot{U}_g + \ddot{U}_b\right)_{1\times 1} - (M_{n\times n})^{-1}\left(C_{n\times n}\dot{U}_{n\times 1} + K_{n\times n}U_{n\times 1}\right) \tag{5}$$

Equation (5) is composed of 3 parts termed (a), (b), and (c) as shown in Eq. (6):

$$\ddot{U}_{n\times 1} = -\underbrace{R_{n\times 1}\left(\ddot{U}_g + \ddot{U}_b\right)_{1\times 1}}_{(a)} - (M_{n\times n})^{-1}\left(\underbrace{C_{n\times n}\dot{U}_{n\times 1}}_{(b)} + \underbrace{K_{n\times n}U_{n\times 1}}_{(c)}\right) \tag{6}$$

Since (a) does not need to be expanded, the expansion of (b) becomes: Eq. (7)

$$\left[C_{n\times n}\,\dot{U}_{n\times 1}\right] = \begin{matrix} \text{i} \\ \text{ii} \\ \\ \\ \text{n} \end{matrix} \begin{bmatrix} C(1,1)*\dot{U}_1 + & C(1,2)*\dot{U}_2 + & C(1,3)*\dot{U}_3 + & \dots & \dots & C(1,n)*\dot{U}_n \\ C(2,1)*\dot{U}_1 + & C(2,2)*\dot{U}_2 + & C(2,3)*\dot{U}_3 + & \dots & \dots & C(2,n)*\dot{U}_n \\ C(3,1)*\dot{U}_1 + & C(3,2)*\dot{U}_2 + & C(3,3)*\dot{U}_3 + & \dots & \dots & C(3,n)*\dot{U}_n \\ \vdots & \vdots & \vdots & \vdots & \vdots & \vdots \\ \vdots & \vdots & \vdots & \vdots & \vdots & \vdots \\ C(n,1)*\dot{U}_1 + & C(n,2)*\dot{U}_2 + & C(n,3)*\dot{U}_3 + & \dots & \cdots & C(n,n)*\dot{U}_n \end{bmatrix} \tag{7}$$

Similarly, expansion of (c) becomes: Eq. (8)

$$\left[K_{n\times n}\,U_{n\times 1}\right] = \begin{matrix} \text{i'} \\ \text{ii'} \\ \\ \\ \text{n'} \end{matrix} \begin{bmatrix} K(1,1)*U_1 + & K(1,2)*U_2 + & K(1,3)*U_3 + & \cdots & \cdots & K(1,n)*U_n \\ K(2,1)*U_1 + & K(2,2)*U_2 + & K(2,3)*U_3 + & \cdots & \cdots & K(2,n)*U_n \\ K(3,1)*U_1 + & K(3,2)*U_2 + & K(3,3)*U_3 + & \cdots & \cdots & K(3,n)*U_n \\ \vdots & \vdots & \vdots & \vdots & \vdots & \vdots \\ \vdots & \vdots & \vdots & \vdots & \vdots & \vdots \\ K(n,1)*U_1 + & K(n,2)*U_2 + & K(n,3)*U_3 + & \cdots & \cdots & K(n,n)*U_n \end{bmatrix} \tag{8}$$

In Eqs. (7) and (8) the notation (i or i'), (ii or ii'), or (n or n') indicates the summation of all elements on the (*i*th or *i*'th), (*ii*th or *ii*'th), or (*n*th or *n*'th) matrix row, respectively. From Eqs. (6)–(8), since matrices $M_{n\times n}$, $C_{n\times n}$, and $K_{n\times n}$ are diagonal (i.e. referring to the idealized multi-degree-of-freedom (MDOF) system shown in Fig. 1f), a new formulation can be obtained for each time-step and each degree of freedom of the superstructure as shown in Eqs. (9)–(11). That is, the equation for the acceleration of the 1st floor $\ddot{U}(1,\ 1)$ can be defined as:

$$\ddot{U}(1,\ 1) = -R(1,\ 1)\left(\ddot{U}_g + \ddot{U}_b\right)_{1\times 1} - \left(i + i'\right)/M(1,\ 1) \tag{9}$$

Similarly, the 2nd floor acceleration as:

$$\ddot{U}(2,\ 1) = -R(2,\ 1)\left(\ddot{U}_g + \ddot{U}_b\right)_{1\times 1} - \left(ii + ii'\right)/M(2,\ 2) \tag{10}$$

And the *n*th floor acceleration as:

$$\ddot{U}(n,\ 1) = -R(n,\ 1)\left(\ddot{U}_g + \ddot{U}_b\right)_{1\times 1} - \left(n + n'\right)/M(n,\ n) \tag{11}$$

(b) The unidirectional substructure motion from Eq. (4) can be rewritten as:

$$\underbrace{\left(R^T_{1\times n} M_{n\times n} R_{n\times 1} + M_{b1\times 1}\right)}_{A_b} \ddot{U}_{b1\times 1} = \underbrace{-\left(R^T_{1\times n} M_{n\times n} \ddot{U}_{n\times 1} + \left(R^T_{1\times n} M_{n\times n} R_{n\times 1} + M_{b1\times 1}\right)\ddot{U}_{g1\times 1} + C_{b1\times 1}\dot{U}_{b1\times 1} + K_{b1\times 1} U_{b1\times 1} + f_{1\times 1}\right)}_{B_b} \tag{12}$$

Then, the base floor acceleration for each time step can be solved as:

$$\ddot{U}_{b1\times 1} = A_b^{-1} B_b \tag{13}$$

When Eq. (3) is written in a simplified form as shown in Eqs. (9)–(11) and (12) as is shown in Eq. (13), any solver capable of handling the stiff system introduced from Eq. (16) will successfully provide accurate solution. Furthermore, the diagonal superstructure mass matrix ($M_{n\times n}$) and stiffness matrix ($K_{n\times n}$) can be used to determine the superstructure damping matrix ($C_{n\times n}$) by using proportional Rayleigh damping formula [31].

$$\left[C_{n\times n}\right] = \alpha_o \left[M_{n\times n}\right] + \alpha_1 \left[K_{n\times n}\right] \tag{14}$$

where the coefficients α_o and α_1 can be determined as shown by [32]. The hysteretic force of LCRB, f, can be modelled using the modified visco-plasticity model (Eq. 15), an extension of Bouc–Wen model [33, 34] owing to its high computational efficiency [35]. With this model, the value for hysteretic restoring force can then be calculated as:

$$f = C_b \dot{U}_b + \alpha K_b U_b + (1-\alpha) f_y Z \tag{15}$$

In Eq. (15), f_y refers to yield force of the bearing, α stands for the ratio of post-yield to pre-yield stiffness; K_b and C_b are stiffness and damping of the bearing, respectively; and Z is a component of Wen's nonlinear model calculated as in Eq. (16), also adopted in [26].

$$\dot{Z} = \left[A\dot{U}_b - \beta\left|\dot{U}_b\right| Z|Z|^{\eta-1} - \tau \dot{U}_b |Z|^{\eta}\right] u_y^{-1} \tag{16}$$

where u_y is yield displacement, β, A and τ are dimensionless parameters defined based on laboratory experiments. η is a constant which controls the transition from elastic to plastic behaviour of the model. In this study, a MATLAB code program was developed to solve all the above equations. Particularly the main part of the developed code includes the solution of the simplified equations shown in Eqs. (9)–(13). Since these equations include the stiff system (Eq. (16)) when calculating the hysteretic force [Eq. (15)], Runge–Kutta fourth-order algorithm was adopted to solve the involved differential equations owing to its high accuracy for such equations [30, 36], assuming a linear variation over a small time step of 0.001 s. The LCRB properties such as K_b and C_b, and u_y were calculated based on following equations [37]:

$$K_b = \left(\frac{2*\pi}{T_b}\right)^2 * \left(M_{\text{sup}} + M_b\right) \tag{17}$$

$$C_b = 2 * \xi_b * \left(M_{\text{sup}} + M_b\right) * w_b \tag{18}$$

$$u_y = \frac{f_y}{K_b}, \quad \xi_b = 0.15, \quad W = \left(M_{\text{sup}} + M_b\right) * g \tag{19}$$

where ξ_b, T_b, g, M_{sup}, W are the bearing damping ratio, bearing natural period, acceleration of gravity ($g = 9.81$),

total mass of superstructure, and the total weight of the structure, respectively.

3.4 Structural Model and Optimization Procedure

To investigate the effectiveness of the seismic isolation, responses of 5-, 10- and 15-storey building models exposed to different types of earthquakes were determined. The adopted structural building models are as previously shown in Fig. 1a–d. These models are simplified as idealized MDOF shear models governed by the equations in Sect. 3.2 and simplified as shown in Sect. 3.3, where the floors are assumed rigid, with massless columns and lumped masses concentrated at each floor level as shown in Fig. 1e, f. The idealized force–displacement relationship adopted for LCRB hysteretic behaviour is shown in Fig. 1g.

Four different types of earthquake ground motions [38] were used as seismic loads in horizontal direction, and their characteristics are as shown in Table 1.

The input parameters characterizing the studied structural models, such as superstructure mass, were calculated based on the dimensions of the models. The stiffness was calculated using finite element method (FEM) [39]. The methodology used in this study is summarized in Fig. 2. The optimal criterion was assured by setting three different conditions: (i) the accuracy condition which was controlled by developing an algorithm for solving the involved equations in a way that the solution leads to the expected idealized force–deflection behaviour already existing in the literature (i.e. Fig. 1g), (ii) the stability condition was assured when the stability of the bearing was achieved (that is, when the hysteretic behaviour or the bearing movement was found centred to ensure the movement of the superstructure was aligned with that of the base structure), (iii) the time instants condition was assured when the storey displacements reached their peaks simultaneously (with a 1 s difference tolerance) to ensure the linear rigid body motion, as previously detailed in the study by [32]. These three conditions incorporate both the isolator and the superstructure responses; hence their satisfaction can imply the effective control of an isolated base and superstructure. In fact, the superstructure responses such as floor accelerations, storey drifts, shear forces, and floor displacements and the isolator responses such as MID, MIF, EDC are all controlled within the three defined conditions. During optimization process, the characteristic parameters of the isolator [26], i.e. isolator period (T_b) and normalized yield strength (F_o), were varied until the above three conditions were satisfied, once satisfied, the corresponding bearing mechanical properties (MPs) were set as optimal and firstly used for determining the substructure and superstructure responses and secondly for determining the shear strains in the elastomer. The MPs considered were the characteristic strength (Q_d), post-yield stiffness ($K_d = \alpha K_b$), elastic stiffness (K_e), effective stiffness (K_{eff}), yield stiffness (K_y), and the yield displacement (u_y). Increasing the isolator period can decrease the isolated superstructure responses and increase the isolator displacement. Also, according to existing studies [24, 26], there exist an optimal value of the Fo that will lead to minimized superstructure responses, such as floor accelerations. Hence, an optimization process based on the F_o and T_b variation is rational. In fact, the restraints of the present study rely on the isolator mechanical properties that satisfy the imposed optimal performance conditions, because the satisfaction of such conditions implies the control of not only the substructure but also the superstructure responses.

4 Results and Discussion

4.1 Base Floor Accelerations

One of the most important responses of an isolated structure is base floor acceleration. In fact, the floor accelerations are a measure of the force transmitted to the superstructure, and hence, the main purpose of seismic isolation is to minimize the accelerations [26]. Typical base floor and maximum base floor accelerations ($\ddot{U}_{\text{bmax}}$) obtained in this study are shown in Fig. 3 and Table 2, respectively.

It can be noted that the base floor accelerations are generally reduced owing to the use of LCRB. However, for Kobe earthquake, the base acceleration is found amplified for a 5-storey building by 18.78%, which may be attributed to the nature of this type of earthquake. Contrary, Duzce earthquake with nearly the same PGA as Kobe is found to significantly reduce the base acceleration for the 5-storey building by 41.33%. Since these two earthquakes only differ from their PGV, it can be inferred that the PGV may be the underlying reason for such huge differences. The frequency content of earthquake is generally measured using PGA/PGV ratio, also known as damage index parameter. Studies have found that earthquakes with lower damage index parameter are likely to amplify structural responses and can cause damage of the bearing due excessive shear strains [9, 40] and may require strict variation limits that are currently not taken into account in the code provisions of ASCE [41]. The fact that Kobe has PGA/PGV = 8.72 while Duzce has PGA/PGV = 12.78 may explain the difference observed for both earthquakes. Hence, it can be noted that both PGA and PGV are important parameters when examining the earthquake severity, and the lower the damage index the higher the negative effects. Besides, strong NF earthquake with higher damage index (Duzce) is observed to reduce the $\ddot{U}_{\text{bmax}}$ for a 5-storey structure more than moderate (10.45%) and long period FF (32.89%) earthquakes; however, the opposite is

Table 1 Characteristics of the earthquakes used in the present study

Earthquake	Comp	PGA (m/s^2)	PGV (m/s)	PGD (m)	Te (s)	Duration (s)	Type
Elcentro	NS	3.11	0.33	0.09	2.88	56.52	LP-M (NF)
Capemembe	NS	1.45	0.43	0.32	3.40	286.65	LP-LD (FF)
Düzce	EW	8.05	0.63	0.12	0.96	55.85	NF
Kobe	NS	8.03	0.92	0.18	1.10	49.93	NF

PGA, *PGV*, and *PGD* are peak ground acceleration, velocity and displacement, respectively, *NF* near-fault, *FF* far-fault, *Te* predominant period, *NS* North–South direction, *EW* East–West direction, *Comp* Component, *M* moderate, *LP* long period, *LD* long duration

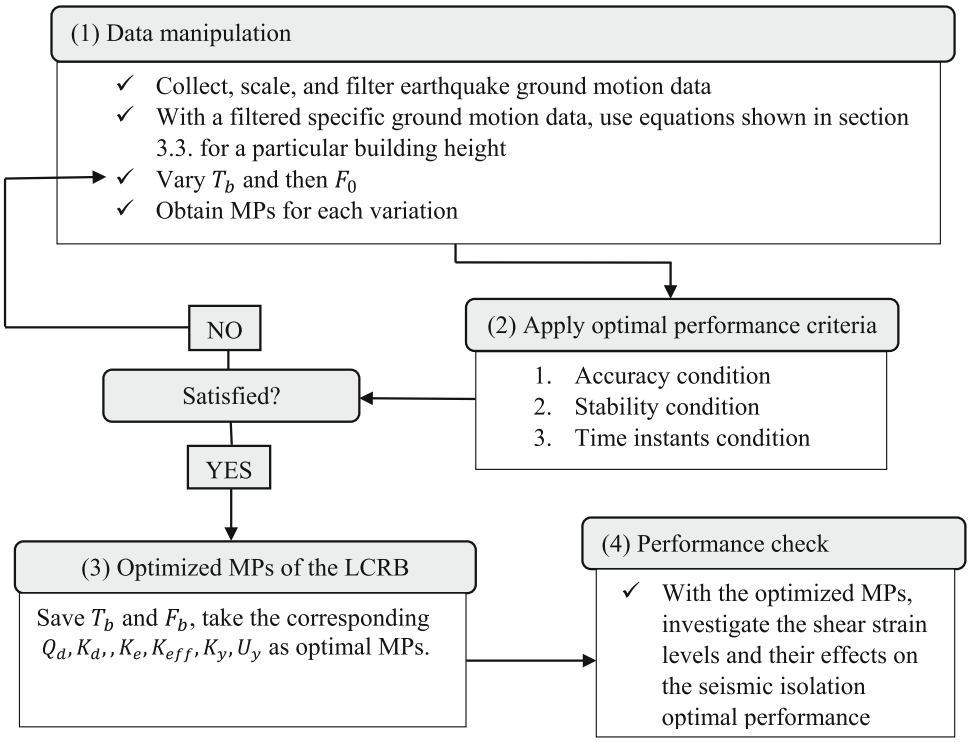


Fig. 2 Summary of the methodology adopted for the evaluation of the seismic isolation performance

observed for a 10-storey structure. For a 15-storey building, NF with higher damage index and FF earthquake tend to reduce the $\ddot{U}_{\text{bmax}}$ more as compared with the remaining earthquakes, and this is in agreement with the findings by [42].

4.2 Force–Displacement Relationship of LCRB Under Various Building Heights and Seismic Loads

Figure 4 shows the force–displacement relations obtained in the present study. When the LCRB is used for low-rise buildings such as the 5-storey model under strong NF motions, the expected hysteretic behaviour is lost, i.e. the behaviour tends to be of elliptic shape rather than bilinear.

Similar results were also observed by [43] where the lead core was not sheared by steel plates due to an applied light vertical load on the bearing, thereby causing the steel plates to bend and the lead to deform into a ball with little damping. For other cases, the bearing shows the expected behaviour by following the idealized force–displacement previously shown in Fig. 1g. Moreover, for all cases, LCRB is found to present stable and centred movements, which indicates its resilience in controlling the movement of the superstructure. Similar response profiles were also experimentally obtained by [2] and analytically by [44].

Comparative perspectives on the resulting MID, EDC and MIF are shown for 5-storey (Fig. 5a), 10-storey (Fig. 5b), and 15-storey (Fig. 5c) buildings, as well as the typical time instants for occurring of the maximum superstructure responses (Fig. 5d). The MID generally decreases with increase in the height of the building (from 10 to 15 storeys), thereby reducing the energy dissipation capacity, except

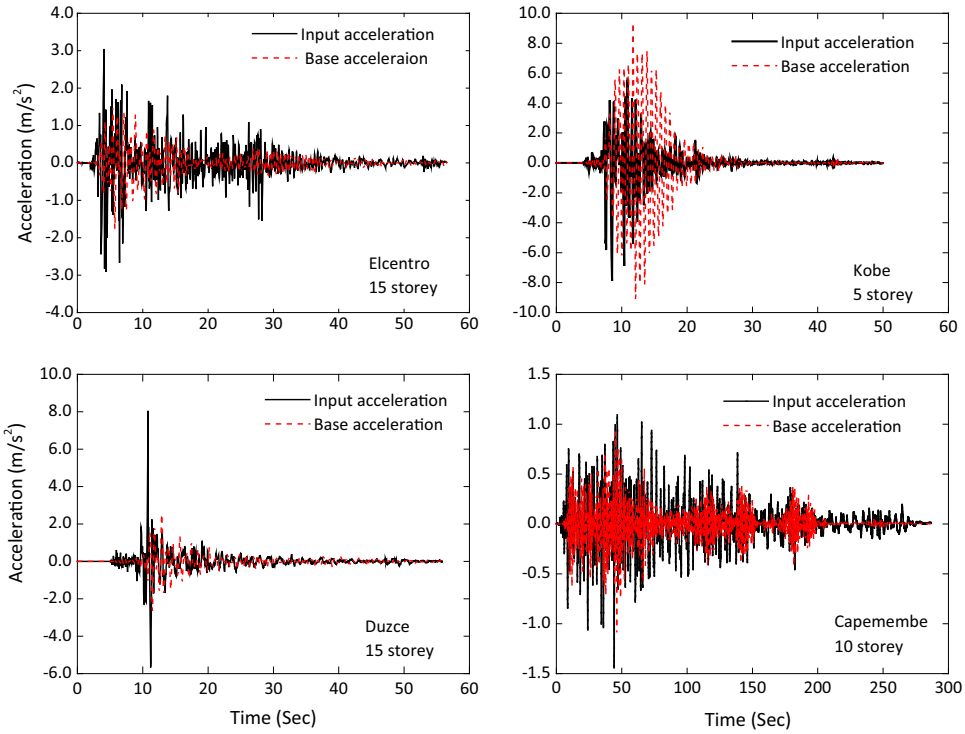


Fig. 3 Earthquake (input) acceleration and base floor acceleration for different building height and earthquake ground motions

Table 2 Variation of maximum base floor acceleration (in %)

Number of storeys	Kobe	Duzce	Elcentro	Capemembe
5	(+)18.78	(−)41.33	(−)10.45	(−)32.89
10	(−)21.00	(−)16.70	(−)35.45	(−)49.88
15	(−)37.51	(−)67.60	(−)45.31	(−)59.84

(+) increase, (−) decrease

for Capemembe (FF) which tends to cause the isolator to increase the dissipation as the height increases (regardless of the number of storeys). MID is found to significantly be affected by the building height where under NF ground motions MID increases from low- to middle-rise building but decreases from middle- to high-rise building; however, it consistently increases from low-to middle- and to-high-rise building under FF ground motion. This shows that the displacement of the isolator is governed by the building height and the type of earthquake ground motion. Besides, MID under NF is found to be significantly large compared to the obtained MID under FF. This was also found by [24] where it was concluded that large displacements due to NF can also cause the instability in the isolation system. Besides, the MID observed under Kobe is nearly twice that under Duzce despite both earthquakes being of NF type and having almost equal PGA. Hence, like the observed trend in the base acceleration, the lower the damage index of a strong NF earthquake the higher the negative effects on the MID.

Furthermore, MIF is observed to vary significantly as the height increases, which is not the case for FF earthquake, where the MIF generally increases as the height increases. It can also be seen that MIF increases as the PGA increases which is in agreement with previous work by [45], except for long-period long-duration earthquake. Also, a comparative perspective between Kobe and Capemembe earthquake for high-rise building (Fig. 5c) indicates that the bearing performs better under FF than under NF by providing much more EDC with less MID and MIF. Finally, the trends in the change of MID, EDC and MIF (see Fig. 5a–c) indicate the differences between NF and FF ground motions for each of the building height. That is, a similar trend where the values for MID, EDC and MIF tend to increase as the PGA increases is found under NF ground motions for all investigated building heights, which is not the case under FF ground motion for high-rise building. Besides, a typical trend showing the time at which the maximum superstructure responses take place (Fig. 5d) indicates that all storeys reach their responses' peaks simultaneously, thereby demonstrating the capacity of the bearing to prevent excessive storey drifts and to lead to a linear motion of the superstructure.

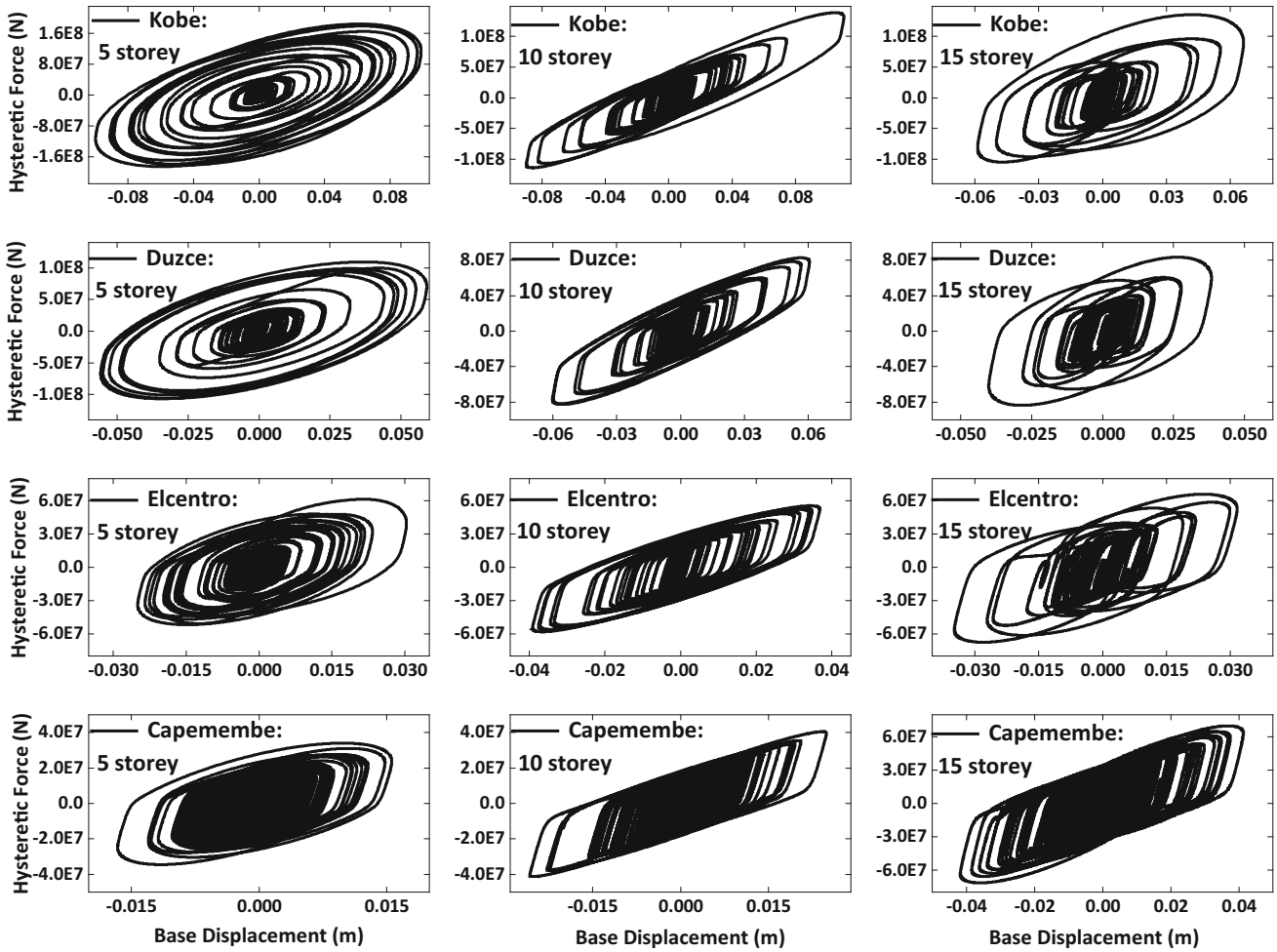


Fig. 4 Hysteretic force–displacement relations for different building heights and ground motions

4.3 Superstructure Storey Displacements

Looking at the maximum top floor displacements (U_{tmax}) resulting from different heights of buildings and different earthquakes in Fig. 6, it can be seen that for all earthquake types the U_{tmax} increases with increase in building height, hence taller buildings tend to displace more as compared to shorter ones, like what was previously found by [18].

The larger displacements observed for tall buildings can be attributed to their longer fundamental periods. Similar trend of distribution of lateral displacements along the height of building were also obtained by [46]. Furthermore, earthquakes with larger PGA are observed to cause larger U_{tmax} than those with less PGA. However, this is not the case for long period long duration earthquakes such as Capemembe which is observed to cause the buildings to experience much larger U_{tmax} than strong NF earthquakes (nearly 2 times larger than Duzce's) despite of its smaller PGA. In fact, Capemembe earthquake possesses many repeated peaks with long pulses over its duration, which may participate in enlarging the top floor displacements through cumulative effects despite the observed lower MID as compared to NF ground motions. Besides, the observed MID and U_{tmax} for NF motions are consistent in a way that higher MID leads to higher U_{tmax}, and the earthquake with lower damage index parameter (Kobe) leads to larger U_{tmax}. The consistency and similar trend for MID and U_{tmax} can indicate the desired harmonized movement between the base and superstructure. Furthermore, comparable values of U_{tmax} are observed for Duzce and Elcentro earthquakes despite of their far different PGAs, hence strongly suggesting that PGA alone cannot characterize earthquake severity. This observation was also previously reported by [32, 44]. In fact, displacement response of isolation system under long duration earthquakes was found to be very closely related to the duration and spectrum rather than PGA [2], and far-field earthquakes have been reported to have particular behaviour and hence cannot be characterized by their PGA as commonly adopted for near-fault ground motions [47, 48].

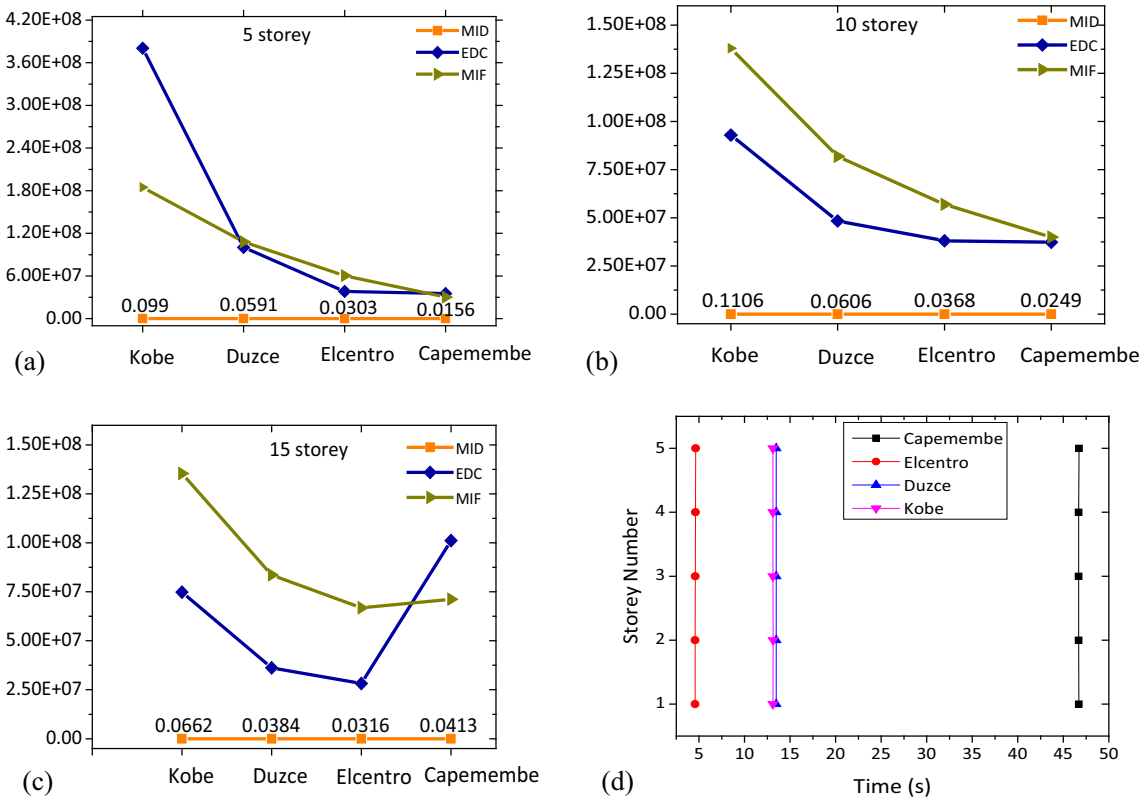


Fig. 5 Variation of LCRB responses for **a** 5-storey, **b** 10-storey and **c** 15-storey buildings, and **d** the time instant for occurrence of superstructure maximum responses under different types of earthquakes (units for MID[m], EDC[J] and MIF[N])

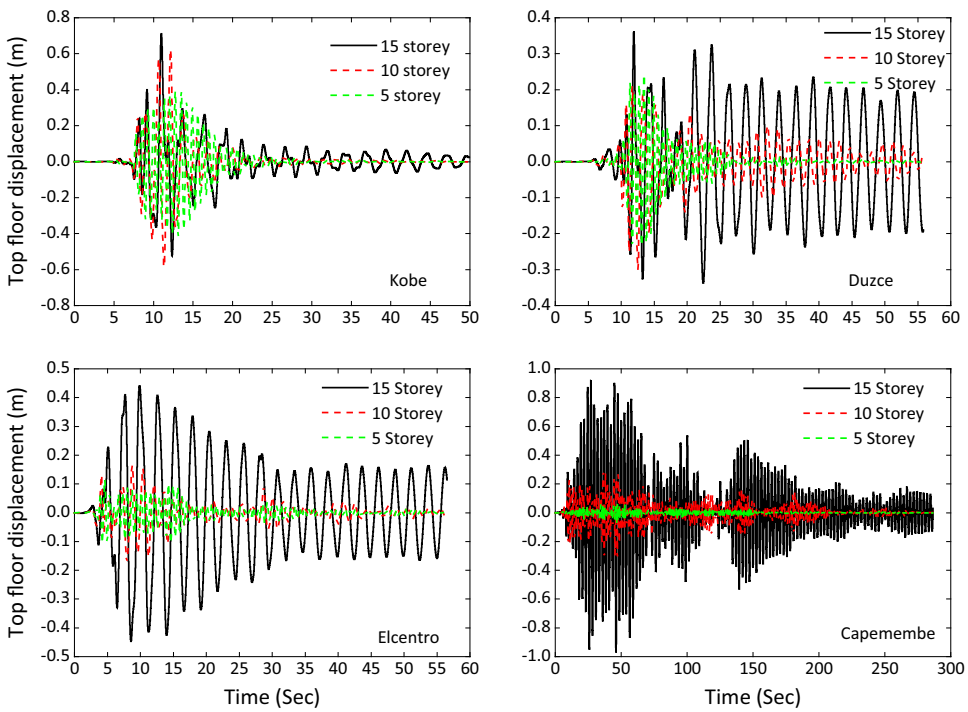


Fig. 6 Typical top floor displacements when LCRB is used for varied building heights under different earthquakes

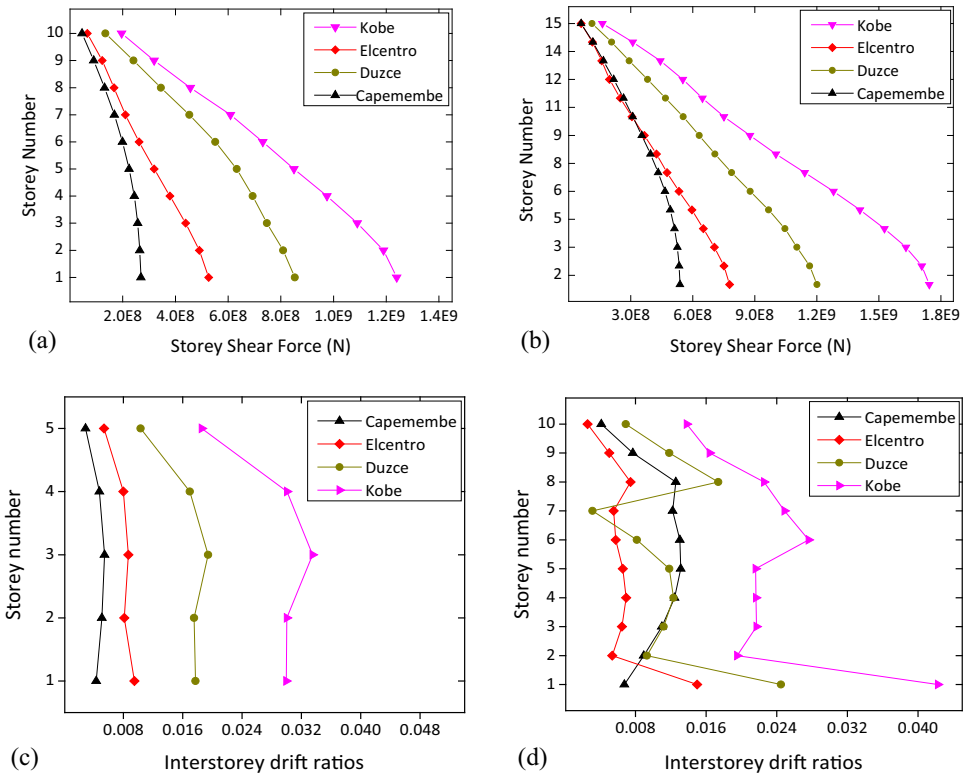


Fig. 7 Typical storey shear force and storey drift profiles for different building heights under different earthquakes: storey shear forces for **a** 10 and **b** 15 storeys, storey drifts for **c** 5 and **d** 10 storeys

4.4 Storey Shear Force and Storey Drift Profiles

Typical storey shear force profiles observed in the present study are shown in Fig. 7a, b. It can clearly be seen that the shear forces decrease as storey levels increase which is generally expected since the maximum inertia force is applied at the top floor of the building where the highest maximum accelerations occur, thereby exerting larger shear forces in the bottom floors as compared to top floors. Further observations indicate that the largest values of shear forces are experienced under Kobe earthquake, followed by Elcentro earthquake. Surprisingly, Duzce earthquake which was expected to present similar behaviour as that of Kobe (because of their nearly equal PGA) is observed to present less shear forces than those from Elcentro earthquake (with much smaller PGA). This strengthens the importance of considering the PGV in conjunction with PGA since it is the only parameter that differentiates Duzce and Kobe earthquakes. On the other hand, Capemembe earthquake shows the expected behaviour by presenting the smallest shear forces due to its smallest PGA.

Typical storey drifts are presented in Fig. 7c, d. The storey drifts increase as the building height increases and are distributed uniformly along the building height for low-rise (Fig. 7c), but the non-uniform distributions are observed for middle (Fig. 7d) and high-rise building categories. Besides, the distribution is dependent on the earthquake type, for example, non-uniform distributions of storey drifts are dominant for strong NF earthquakes such as Kobe and Duzce, particularly the former causes sharp change in the distribution between the 5th and 6th storey and the latter between the 7th and 8th storey for the examined 10-storey building (see Fig. 7d). Nevertheless, the maximum drifts are kept at the first floor as expected. Besides, the effect of lower damage index earthquake (Kobe) again shows higher severity with larger storey drifts than those from the higher damage index (Duzce).

Similar trend of distribution of shear forces along the height of the considered buildings were also obtained by [46], and in experimental studies by [49, 50]. The observed increase of shear forces as the building height increases has also been observed by other researchers [18], but for only one building height. Besides, controlling the storey drifts is necessary mainly to limit damage to non-structural components such as partitions, glass window and facades. Referring to ASCE 7–16 standard [41], the storey drift limits will depend on the type and location of the building (i.e. based on the risk category I up to IV). According to the above standard, the drift limits for buildings up to four storeys (if located in category I or II) would be calculated as 0.025 h_{sx}, where h_{sx} is the storey height below level x. However, ASCE 7–16 does not provide the drifts requirements for buildings that fall into low-rise, middle-rise and high-rise categories, hence the storey drifts obtained in this study cannot be compared with

Table 3 MID, EDC and MIF percentage differences between LCRB alone and LCRB coupled with FVD

	Difference in MID (%)	Difference in EDC (%)	Difference in MIF (%)
5 Storeys			
Kobe	(−)8.59	(+)88.44	(+)68.10
Duzce	(−)10.66	(+)100.29	(+)86.59
Elcentro	(−)19.14	(+)87.83	(+)107.19
Capemembe	(−)22.44	(+)61.26	(+)135.81
10 storeys			
Kobe	(−)12.21	(−)5.84	(−)6.16
Duzce	(−)16.83	(−)6.00	(−)10.05
Elcentro	(−)38.04	(−)16.10	(−)1.22
Capemembe	(−)10.84	(+)45.26	(−)16.27
15 storeys			
Kobe	(−)25.38	(+)44.20	(+)54.29
Duzce	(−)32.29	(+)118.60	(+)67.35
Elcentro	(−)21.84	(+)37.29	(+)51.28
Capemembe	(−)7.75	(+)104.14	(+)65.30

(+) increase, (−) decrease

the requirements in the ASCE 7–16 but can help in improving the existing standards, such as the ASCE 7–16.

4.5 Effects of Coupling LCRB with Nonlinear Fluid Viscous Damper

Shear strains in the elastomer: referring to the recommendations from EN 1337-3 [23], shear strains (ε_{qE}) due to earthquake-imposed horizontal displacement can be calculated as:

$$\varepsilon_{qE} = d_{bd}/T_q \tag{20}$$

where d_{bd} is the earthquake-imposed design displacement and T_q is the total thickness of the elastomer active during shear occurrence.

As previously introduced in Sect. 1, many studies and different existing code provisions controversially report the maximum allowable shear strains in the elastomer; however, most of the studies agree on limiting the shear strains to 100%, e.g. EN 1337-3 [23] and other available works [12, 17]. Hence, the 100% elastomer shear strain is set as a reference in the present study. Referring to the MID previously presented in Fig. 5 (when using a small size LCRB with total elastomer thickness of 60 mm and height of 166.88 mm, previously investigated by [51]), the shear strains calculated using Eq. (20) under strong motions such as Kobe can be very high and exceed the recommended values in the EN1337-3 [23] for all the studied buildings. Additionally, the calculated strains may exceed the value that was reported by [10] to cause tensile stresses larger than 5G (i.e. 125%), particularly for the studied 5- and 10-storey buildings. In fact, near-fault earthquakes were reported to cause hardening of the LCRB as a result of excessive tensile stresses, thereafter leading to large maximum accelerations [52]. Such large tensile stresses in the elastomer may also cause the development of bearing cracks and lead to buckling and rupture, thereby resulting in poor performance of the isolation system [10, 32]; and can also cause tension [2] and softening in vertical direction [53]. Therefore, using LCRB alone in the isolation system under strong NF ground motions may, in some cases, be ineffective. In order to reduce the excessive shear strains in the elastomer, previous studies have suggested coupling the LCRB with FVD [54]. The coupling of bearings with FVD was reported to significantly reduce the unwanted larger displacements that result from NF earthquakes by a number of researchers [46, 54, 55]. Another possible strategy is to limit the normalized yield strength of the bearing in the range 10–15% [24], 10–14% [25], but these ranges are generally comparable to those adopted in the present work. In this regard, this study attempted to couple LCRB with nonlinear FVD governed by Eq. (21).

$$F = C\left|\dot{U}_b\right|^{\alpha}\mathrm{sgn}\left(\dot{U}_b\right) \tag{21}$$

where C is damping coefficient, α is in the range of [0.5–1.0]. The nonlinear FVD and its force (F)-displacement relationship, are shown in Fig. 8.

The hysteretic responses of different building heights under various earthquake types are shown in Fig. 9. A reduction of MID and increase of EDC is generally achieved owing to the hybrid of LCRB and FVD. Also, like what was previously observed for the sole use of LCRB, the resulting hysteretic shapes for the hybrid are centred and stable, thereby showing promising substructure movements, which also implies the control of the movement of the superstructure. Besides, the expected ideal force–displacement relation (Fig. 8b) of FVD is generally reflected in the obtained results. Furthermore, the elliptic shape, previously observed when using LCRB alone for low-rise 5-storey building, is again reflected after addition of FVD, particularly for strong near-fault ground motions.

Looking at the Fig. 10, the addition of FVD has no adverse effect on the trends in the change of MID, EDC and MIF as it results in the same trends as those observed when LCRB is used alone. In fact, like what is observed with the sole use of LCRB, an increasing trend of MID, EDC and MIF values is found as the PGV increases for NF ground motions, i.e. the higher the values the higher the PGV of the NF ground motions for all investigated building heights (Fig. 10a–c); however, such an increasing trend is lost under FF ground

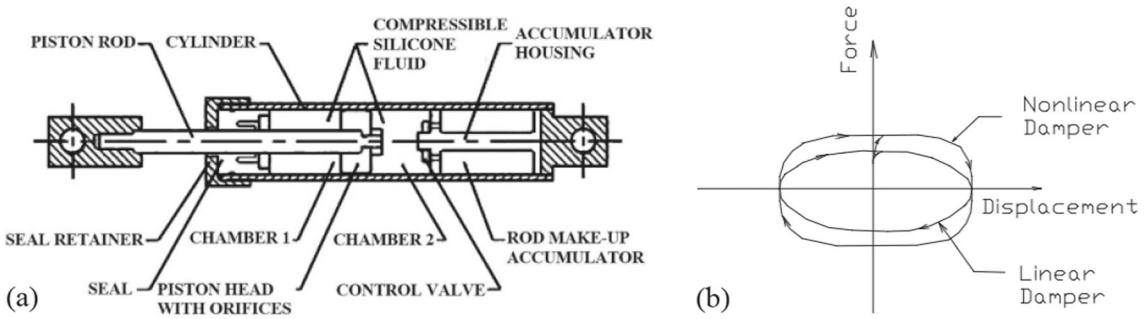


Fig. 8 **a** Fluid viscous damper and **b** ideal force–displacement relation [35]

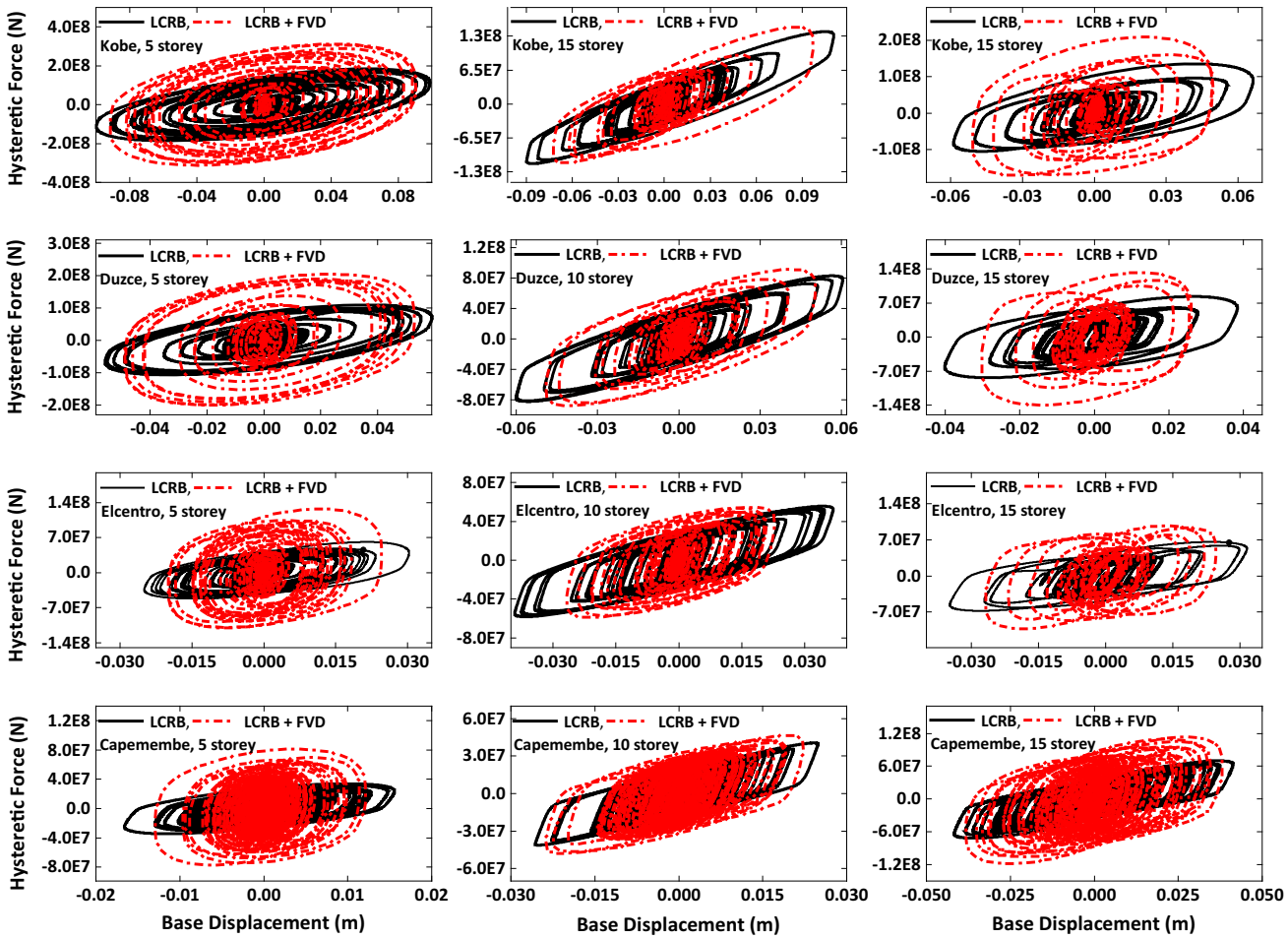


Fig. 9 Hysteretic force–displacement relations using LCRB, and LCRB coupled with FVD, for different building height under various earthquake types

motion for the case of 15-storey building (Fig. 10c), which may be attributed to the FF ground motion characteristics.

To facilitate the examination of the results from Fig. 10, the percentage differences between the sole use of LCRB and the coupling of LCRB with FVD are presented in Table 3. Overall, regardless of the ground motion type and building height, addition of FVD is observed to result in a positive effect on reducing the MID, and a higher positive effect is observed for NF ground motion with higher damage index than for that with lower index. Furthermore, addition of FVD for low- and high-rise building can significantly increase EDC regardless of the earthquake type; however, it can negatively lead to a higher increase in MIF for low-rise building than for high-rise building thereby indicating that more benefits of adding FVD can be reached when the hybrid is adopted for high-rise building.

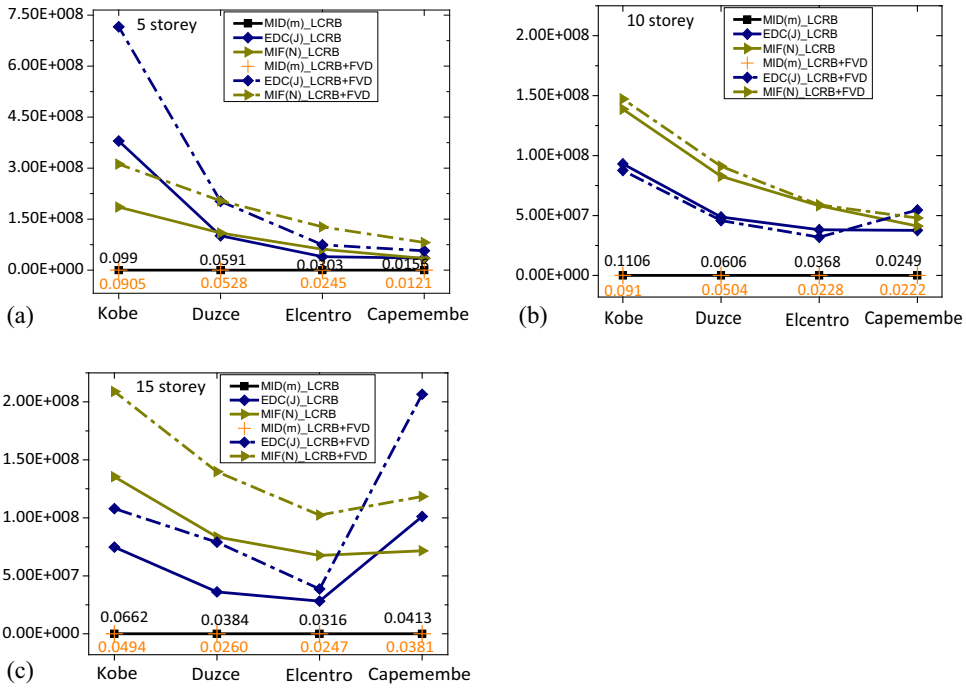


Fig. 10 Effects of coupling LCRB with nonlinear FVD for different building heights and different ground motions: Variation of MID, EDC and MIF for **a** 5-storey, **b** 10-storey, **c** 15-storey buildings

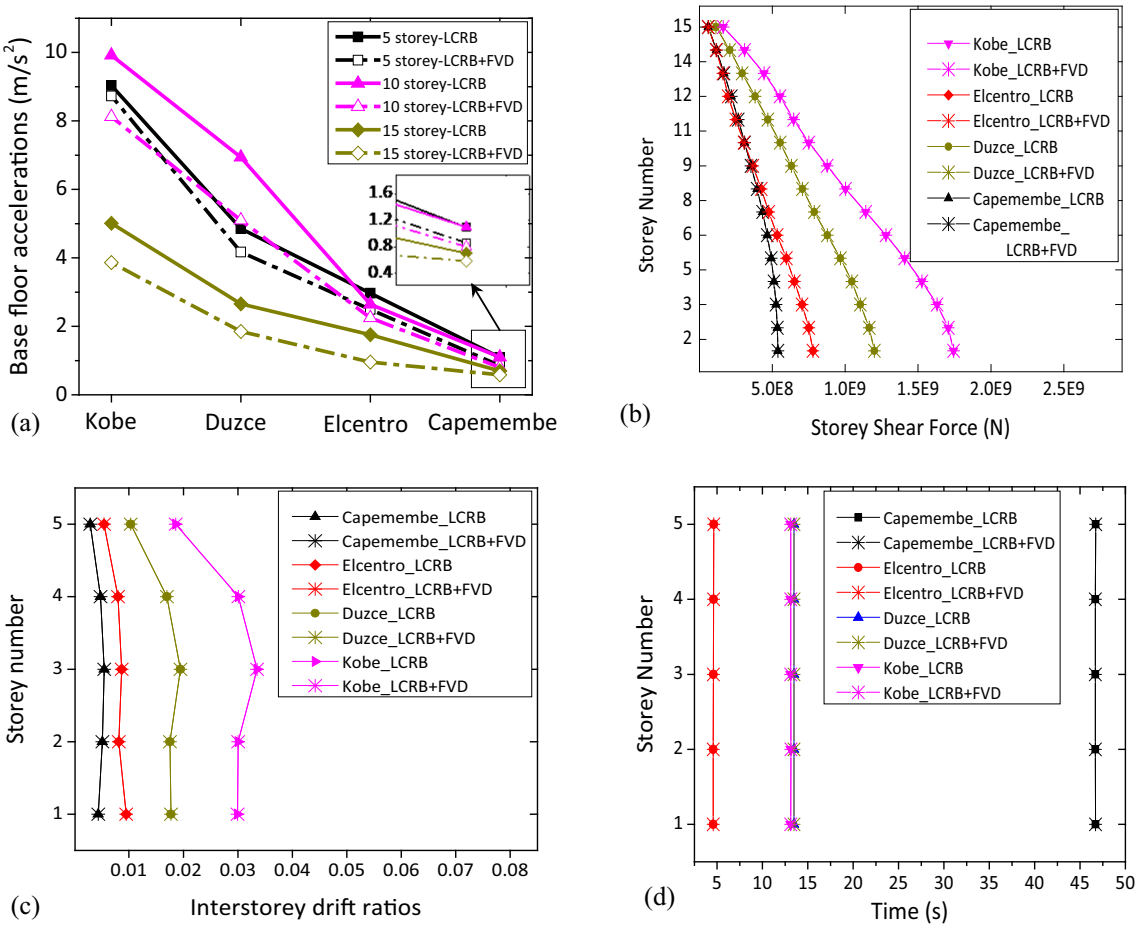


Fig. 11 Effects of coupling LCRB with nonlinear FVD for different building heights and different ground motions: **a** variation of base floor acceleration; **b** variation storey shear forces; **c** variation of storey drifts, and **d** the time instant for occurrence of superstructure maximum responses

For middle-rise building, it can be noted that the addition of FVD under NF earthquakes will reduce the MID and slightly reduce both the EDC and MIF, while under FF ground motion the FVD will positively affect MID, EDC and MIF thereby leading to effective control of the base isolation system. Particularly, the hybrid of LCRB and FVD for middle-rise building is observed to lead to the most promising results under FF ground motion by reducing both MID by 10.84% and MIF by 16.27% while substantially increasing the EDC by 45.26%.

Effects of coupling LCRB and FVD on the base floor acceleration are shown in Fig. 11a. For the examined 5-storey, 10-storey, and 15-storey buildings, the addition of FVD under Duzce earthquake can reduce the base floor acceleration by 14.18%, 26.50%, and 31.04%, respectively; under Kobe earthquake by 3.40%, 18.12%, and 19.06%, respectively; under Elcentro earthquake by 16.38%, 38.87%, and 44.12%, respectively; and under Capemembe earthquake by 21.73%, 27.28%, and 16.60%, respectively. Overall, when LCRB is coupled with FVD, the base floor acceleration decreases in all cases, thanks to the addition of the FVD. Also, the base acceleration is observed to decrease more as the building height increases regardless of the type of the seismic ground motion, which indicates that the hybrid may be thought to perform better for high-rise buildings when considering the reduction of the base floor acceleration. On the other hand, the hybrid is found to have no effects on the superstructure responses such as storey shear forces (Fig. 11b) and storey drifts (Fig. 11c), and the time for the occurring of the maximum superstructure responses (Fig. 11d), which shows the benefits of adding FVD to improve the substructure responses without adversely affecting the superstructure responses.

The reduction of MID for NF ground motions without adversely affecting the superstructure responses, has also been observed in the study by [55]. However, this study additionally shows that MID and base accelerations can be reduced by the hybrid under both NF and FF ground motion. Besides, the MID reduction depends not only on the type of ground motion but also on the height of the building. That is, the hybrid is observed to significantly reduce the MID even for FF ground motions for all investigated building heights, but the benefits decrease as the building height increases. Particularly, the benefits are more dominant for middle-rise buildings when considering the combined effects of all the substructure responses (i.e. MID, EDC, MIF, and base acceleration).

To examine the variations of the shear strains in the elastomer of bearing for the case of LCRB, and the hybrid of LCRB and nonlinear FVD, Table 4 and Fig. 12 are presented. Looking at the summarized peak responses in Table 4, the hybrid is clearly observed to reduce the shear strains. The level of the benefits from the hybrid strongly depends on the building height and the type of ground motion. In fact, the highest benefits are found under moderate NF earthquake for middle-rise building with 37.70% reduction, followed by strong NF motion with higher damage index for high-rise building with 32.34% reduction. Besides, Fig. 12 shows that the effectiveness of adding nonlinear FVD becomes significant as the number of stories increases under strong NF ground motions while the opposite is observed under FF long-period long-duration motion.

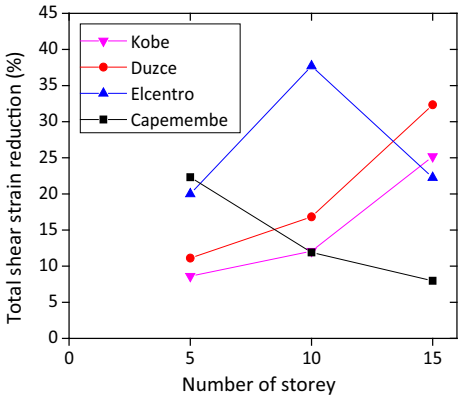


Fig. 12 Effects of coupling LCRB with nonlinear FVD: reduction of shear strains owing to the hybrid use of LCRB and nonlinear FVD

The reduced shear strains under Kobe earthquake are smaller than the EN 1337-3 [23] recommended values only for the high-rise 15-storey building while the strains for the 5- and 10-storey buildings are still higher than those recommended (see Table 4). This has also been observed in the previous study [26], where the earthquakes (taken from 1989 Loma Prieta and the 1979 Imperial Valley) caused large isolator displacements, which was attributed to their dominant spectral characteristics and their proximity to the isolator characteristic frequency. In this regard, the present work suggests that for strong NF motions with low damage index parameter, such as Kobe, using small size bearing may not be promising even when the FVD is added; however, it can be inferred that the use of bigger size bearing can result in smaller shear strains. However, this needs further investigation for confirmation.

5 Conclusions and Recommendations

In this study, effects of building height and earthquake ground motion type on the optimal lead core rubber bearing (LCRB) performance (and the performance of the hybrid of the bearing with nonlinear fluid viscous damper) were investigated. An approach capable of incorporating an optimal criterion that considers the conditions that lead to controlled substructure and superstructure responses was developed. With this approach, the substructure and superstructure responses of

Table 4 Variation of shear strain levels in the elastomer of LCRB

	MID (m) with LCRB	TSS (%)	MID (m) with LCRB + FVD	TSS (%)	Decrease (%)
5 Storeys					
Kobe	0.099	165	0.0905	150.8	8.61
Duzce	0.0591	99	0.0528	88	11.11
Elcentro	0.0303	51	0.0245	40.8	20.00
Capemembe	0.0156	26	0.0121	20.2	22.31
10 Storeys					
Kobe	0.1106	184	0.0971	161.8	12.07
Duzce	0.0606	101	0.0504	84	16.83
Elcentro	0.0368	61	0.0228	38	37.70
Capemembe	0.0249	42	0.0222	37	11.90
15 Storeys					
Kobe	0.0662	110	0.0494	82.3	25.18
Duzce	0.0384	64	0.026	43.3	32.34
Elcentro	0.0316	53	0.0247	41.2	22.26
Capemembe	0.0413	69	0.0381	63.5	7.97

MID Maximum isolator displacement, *FVD* fluid viscous damper, *TSS* total shear strains

isolated three building models, categorized as low-rise (5-storey), middle rise (10-storey), and high-rise (15-storey) buildings, exposed to different seismic ground motions, were assessed. The key findings from this work are summarized below.

(i) The investigated buildings are generally found to benefit from the LCRB by presenting promising substructure and superstructure responses. The performance of the LCRB is found to significantly depend on the type of the earthquake and the building height. For example, the higher the building height the higher the maximum isolator displacement under far-fault earthquakes, which is not the case under near-fault motions. Furthermore, the superstructure responses become higher as the building height increases but the variation strongly depend on the type of the ground motion, where for example, far-fault long period long duration earthquake is observed to lead to substantially larger top floor displacements than near-fault earthquakes. Furthermore, negative effects on the responses of the investigated buildings are generally found under strong near-fault ground motion with lower damage index parameter, while the ground motion with higher index mostly leads to positive effects.

(ii) To avoid the excessive shear strains resulting from the sole use of LCRB, the hybrid of LCRB with FVD is found to be promising by reducing the LCRB displacement and base floor acceleration without adverse effects on the superstructure responses. However, for strong near-fault earthquakes with lower damage index parameter, the obtained shear strains are still higher than those recommended in the code provisions. Besides, the shear strain reductions strongly depend on the combined effect of building height and earthquake type, the higher the height the higher the reductions for strong near-fault and the lower the reductions for far-fault ground motions. In general, the benefits from the hybrid are dominant for middle- and high-rise building. The hybrid can notably lead to effective control of MID, EDC, and MIF for middle-rise building under far-fault earthquake.

(iii) *Recommendations* The results from this work are pertinent to the investigated building models with symmetric structural layout, further studies on the effect of earthquake type and building height variation (e.g. building models with symmetric and/or asymmetric layout) when using the LCRB coupled with nonlinear FVD can be recommended as such studies are generally scarce in the existing literature. Also, in the present study, only a few earthquake ground motions are adopted. Hence, further studies with a wide range of the earthquakes (e.g. those with extended shaking and with forces causing excessive torsion and compression) are recommended to have an advanced understanding on the behaviour of the base isolation system for different building heights.

Acknowledgements Authors would like to sincerely acknowledge the administrative and technical support from the University of Rwanda,

College of Science and Technology leadership, provided until the completion of this work. Furthermore, this work was partly financed by FCT/MCTES through national funds (PIDDAC) under the R&D Unit Institute for Sustainability and Innovation in Structural Engineering (ISISE), under reference UIDB/04029/2020, and under the Associate Laboratory Advanced Production and Intelligent Systems ARISE under reference LA/P/0112/2020. This work was also financed by national funds through FCT - Foundation for Science and Technology, under grant agreement [DFA/BD/08403/2021] attributed to the 1st author.

Funding Open access funding provided by FCT|FCCN (b-on).

Open Access This article is licensed under a Creative Commons Attribution 4.0 International License, which permits use, sharing, adaptation, distribution and reproduction in any medium or format, as long as you give appropriate credit to the original author(s) and the source, provide a link to the Creative Commons licence, and indicate if changes were made. The images or other third party material in this article are included in the article's Creative Commons licence, unless indicated otherwise in a credit line to the material. If material is not included in the article's Creative Commons licence and your intended use is not permitted by statutory regulation or exceeds the permitted use, you will need to obtain permission directly from the copyright holder. To view a copy of this licence, visit http://creativecommons.org/licenses/by/4.0/.

References

1. Shinozuka, M.; Chaudhuri, S.R.; Mishra, S.K.: Shape-memory-alloy supplemented lead rubber bearing (SMA-LRB) for seismic isolation. Probabilistic Eng. Mech. **41**, 34–45 (2015). https://doi.org/10.1016/j.probengmech.2015.04.004
2. Zhan, J.D.; Li, X.T.; Li, Y.: Comparative study on nonlinear earthquake response of girder isolated bridges with LRB and model shaking table test. Adv. Mater. Res. **706–708**, 472–477 (2013). https://doi.org/10.4028/www.scientific.net/AMR.706-708.472
3. Pokhrel, A.; Li, J.; Li, Y.; Maksis, N.; Yu, Y.: Comparative studies of base isolation systems featured with lead rubber bearings and friction pendulum bearings. Appl. Mech. Mater. **846**, 114–119 (2016). https://doi.org/10.4028/www.scientific.net/AMM.846.114
4. Han, J.; Kyu, M.; Choi, I.: Experimental study on seismic behavior of lead-rubber bearing considering bi-directional horizontal input motions. Eng. Struct. **198**, 109529 (2019). https://doi.org/10.1016/j.engstruct.2019.109529
5. Gupta, P.K.; Ghosh, G.: Effect of bi-directional excitation on a curved bridge with lead rubber bearing. Mater. Today Proc. **44**, 2239–2244 (2021). https://doi.org/10.1016/j.matpr.2020.12.362
6. Mkrtychev, O.V.; Dzhinchvelashvili, G.A.; Bunov, A.A.: Study of lead rubber bearings operation with varying height buildings at earthquake. Procedia Eng. **91**, 48–53 (2014). https://doi.org/10.1016/j.proeng.2014.12.010
7. Nagarajaiah, S.; Xiaohong, S.: Response of base-isolated USC hospital building in Northridge earthquake. J. Struct. Eng. **126**, 1177–1186 (2000). https://doi.org/10.1061/(ASCE)0733-9445(2000)126:10(1177)
8. Naeim, F.; Kelly, J.M.: Design of seismic isolated structures, 1st edn. Wiley, New York (1999)
9. Choun, Y.S.; Park, J.; Choi, I.K.: Effects of mechanical property variability in lead rubber bearings on the response of seismic isolation system for different ground motions. Nucl. Eng. Technol. **46**, 605–618 (2014). https://doi.org/10.5516/NET.09.2014.718
10. Kalfas, K.N.; Mitoulis, S.A.; Katakalos, K.: Numerical study on the response of steel-laminated elastomeric bearings subjected to variable axial loads and development of local tensile stresses. Eng. Struct. **134**, 346–357 (2017). https://doi.org/10.1016/j.engstruct.2016.12.015
11. Kalfas, K.N.; Mitoulis, S.A.: Performance of steel laminated rubber bearings subjected to combinations of axial loads and shear strains. Procedia Eng. **199**, 2979–2984 (2017). https://doi.org/10.1016/j.proeng.2017.09.533
12. Kumar, M.; Whittaker, A.S.; Constantinou, M.C.: Experimental investigation of cavitation in elastomeric seismic isolation bearings. Eng. Struct. **101**, 290–305 (2015). https://doi.org/10.1016/j.engstruct.2015.07.014
13. Kumar, M.; Whittaker, A.S.; Constantinou, M.C.: An advanced numerical model of elastomeric seismic isolation bearings. Earthq. Eng. Struct. Dyn. (2014). https://doi.org/10.1002/eqe.2431
14. Hamaguchi, H.; Samejima, Y.; Kani, N.: A study of aging effect on rubber bearings after about twenty years in use. In: 11th World Conference on Seismic Isolation, Energy. Dissipation and Active Vibration Control of Structures, Guangzhou, China (2009)
15. Shimoda, I.; Masayoshi, I.; Mochimaru, M.; Miyazaki, M.; Sakuraba, S.; Masuda, K.; Wake, T.: Survey of aging for LRB of a base-isolated building completed 15 years ago. Am. Soc. Mech. Eng. Press. Vessel. Pip. Div. PVP. **486**, 1–6 (2004). https://doi.org/10.1115/PVP2004-2926
16. AASHTO, American Association of State Highway and Transportation Officials: Guide Specifications for Seismic Isolation Design. 4th edn., Washington (2014)
17. Eem, S.; Hahm, D.: Large strain non-linear model of lead rubber bearings for beyond design basis earthquakes. Nucl. Eng. Technol. **51**, 600–606 (2019). https://doi.org/10.1016/j.net.2018.11.001
18. Tavakoli, H.R.; Naghavi, F.; Goltabar, A.R.: Dynamic responses of the base-fixed and isolated building frames under far- and near-fault earthquakes. Arab. J. Sci. Eng. **39**, 2573–2585 (2014). https://doi.org/10.1007/s13369-013-0891-8
19. Buckle, I.; Yen, W.; Marsh, L.; Monzon, E.: Implications of bridge performance during great east Japan earthquake for U.S. seismic design practice. In: Proceedings of the International Symposium on Engineering Lessons Learned from the 2011 Gt. Eat Japan Earthquake, Tokyo, Japan, pp. 1363–1374 (2012)
20. Uno, Y.; Sumimura, T.; Kanai, H.: Research regarding the horizontal characteristics of various elastomeric bearings under tension influence (written in Japanese). J. Earthq. Eng. **27**, 1–4 (2003)
21. Yang, Q.R.; Liu, W.G.; Ph, D.; He, W.F.; Feng, D.M.; Ph, D.: Tensile stiffness and deformation model of rubber isolators in tension and tension shear states. J. Eng. Mech. (2010). https://doi.org/10.1061/(ASCE)EM.1943-7889.0000007
22. BS EN 15129: 2009: Anti-seismic devices. BSI British Standards (2010)
23. EN 1337–3: Structural bearings—Part 3: elastomeric bearings, p. 2005. European Committee for Standardization, Brussels (2005)
24. Jangid, R.S.: Optimum lead-rubber isolation bearings for near-fault motions. Eng. Struct. **29**, 2503–2513 (2007). https://doi.org/10.1016/j.engstruct.2006.12.010
25. Rong, Q.: Optimum parameters of a five-story building supported by lead-rubber bearings under near-fault ground motions. J. Low Freq. Noise Vib. Active Control (2019). https://doi.org/10.1177/1461348419845829
26. Das, S.; Gur, S.; Mishra, S.K.; Chakraborty, S.: Optimal performance of base isolated building considering limitation on excessive isolator displacement. Struct. Infrastruct. Eng. **11**, 904–917 (2015). https://doi.org/10.1080/15732479.2014.921716
27. Liao, W.I.; Loh, C.H.; Lee, B.H.: Comparison of dynamic response of isolated and non-isolated continuous girder bridges subjected to near-fault ground motions. Eng. Struct. **26**, 2173–2183 (2004). https://doi.org/10.1016/j.engstruct.2004.07.016

28. China National Standards. Code for Design of Civil Building (GB50352-2005). China Architecture & Building Press, Beijing, China (2005)
29. Tsopelas, P.; Nagarajaiah, S.; Constantinou, M.C.; Reinhorn, A.M.: 3D-BASIS-M: nonlinear dynamic analysis of multiple building base isolated structures (1991)
30. Ramos, H.; Vigo-Aguiar, J.: A fourth-order Runge–Kutta method based on BDF-type Chebyshev approximations. J. Comput. Appl. Math. **204**, 124–136 (2007). https://doi.org/10.1016/j.cam.2006.04.033
31. Chopra, A.K.: Dynamics of Structures: Theory and Applications to Earthquake Engineering, 4th edn. Prentice Hall, California (2012)
32. Dushimimana, A.; Niyonsenga, A.A.; Decadjevi, G.J.; Kathumbi, L.K.: Effects of model-based design and loading on responses of base-isolated structures. Mag. Civ. Eng. **92**, 142–154 (2019). https://doi.org/10.18720/MCE.92.12
33. Bouc, R.: Forced vibration of mechanical systems with hysteresis. In: Proceedings of the Fourth Conference on Nonlinear Oscillations, Prague, Czechoslovakia (1967)
34. Wen, Y.K.: Method for random vibration of hysteretic systems. J. Eng. Mech. Div. ASCE. **102**, 249–263 (1976)
35. Cimellaro, G.P.; Nagarajaiah, S.; Kunnath, S.K.: Computational Methods, Seismic Protection, Hybrid Testing and Resilience in Earthquake Engineering. Springer, Cham (2015) https://doi.org/10.1007/978-3-319-06394-2††
36. Tay, K.G.; Kek, S.L.; Cheong, T.H.; Abdul-Kahar, R.; Lee, M.F.: The fourth order Runge–Kutta spreadsheet calculator using VBA programing for ordinary differential equations. Procedia Soc. Behav. Sci. **204**, 231–239 (2015). https://doi.org/10.1016/j.sbspro.2015.08.145
37. Dushimimana, A.; Nzamurambaho, F.; Shyaka, E.; Niyonsenga, A.A.: Optimum performance of isolation system for medium rise buildings subject to long period ground motions. Int. J. Appl. Eng. Res. **13**, 16342–16350 (2018)
38. University of California, Pacific Earthquake Engineering Research Center (PEER) NGA: Ground Motion Database (2013). https://peer.berkeley.edu/peer-strong-ground-motion-databases Accessed 20 June 2018
39. Kasimzade, A.A.; Dushimimana, A.; Tuhta, S.; Atmaca, G.; Günday, F.; Pfidze, K.; Abrar, O.: A comparative study on effectiveness of using Horasan Mortar as a pure friction sliding interface material. Eur. J. Eng. Res. Sci. **4**, 64–69 (2019). https://doi.org/10.24018/ejers.2019.4.2.1166
40. Dicleli, M.; Karalar, M.: Optimum characteristic properties of isolators with bilinear force–displacement hysteresis for seismic protection of bridges built on various site soils. Soil Dyn. Earthq. Eng. **31**, 982–995 (2011). https://doi.org/10.1016/j.soildyn.2011.03.005
41. ASCE 7-16: Minimum design loads for buildings and other structures (2013)
42. Anajafi, H.; Poursadr, K.; Roohi, M.; Santini-Bell, E.: Effectiveness of seismic isolation for long-period structures subject to far-field and near-field excitations. Front. Built Environ. **6**, 1–17 (2020). https://doi.org/10.3389/fubil.2020.00024
43. Robinson, H.: Lead-rubber hysteretic bearings suitable for protecting structures during earthquakes. Earthq. Eng. Struct. Dyn. **10**, 593–604 (1982)
44. Dushimimana, A.; Singirankabo, E.; Kathumbi, L.K.: Effective seismic response control of buildings with sliding bearings. Mag. Civ. Eng. **89**, 124–141 (2020). https://doi.org/10.34910/MCE.108.9
45. Jian, F.; Xiaohong, L.; Yanping, Z.: Optimum design of lead-rubber bearing system with uncertainty parameters. Struct. Eng. Mech. **56**, 959–982 (2015). https://doi.org/10.12989/sem.2015.56.6.959
46. Ganji, M.; Kazem, H.: Comparing seismic performance of steel structures equipped with viscous dampers and lead rubber bearing base isolation under near-field earthquake. Civ. Eng. J. **3**, 124–136 (2017). https://doi.org/10.28991/cej-2017-00000079
47. Cao, V.V.; Ronagh, R.H.: Correlation between seismic parameters of far-fault motions and damage indices of low-rise reinforced concrete frames. Soil Dyn. Earthq. Eng. **66**, 102–112 (2014). https://doi.org/10.1016/j.soildyn.2014.06.020
48. Kodakkal, A.; Saha, S.K.; Sepahvand, K.; Matsagar, V.A.; Duddeck, F.; Marburg, S.: Uncertainties in dynamic response of buildings with non linear base- isolators. Eng. Struct. **197**, 109423 (2019). https://doi.org/10.1016/j.engstruct.2019.109423
49. Sano, T.; Shirai, K.; Yoshida, O.; Nishikage, T.: Assessment of a seismic tuned mass damper with friction fail-safe mechanism for the vibration control of high-rise buildings. Struct. Control Heal. Monit. **28**, 1–22 (2021). https://doi.org/10.1002/stc.2831
50. Kang, B.S.; Li, L.; Ku, T.W.: Dynamic response characteristics of seismic isolation systems for building structures. J. Mech. Sci. Technol. **23**, 2179–2192 (2009). https://doi.org/10.1007/s12206-009-0437-x
51. Sanchez, J.; Masroor, A.; Mosqueda, G.; Ryan, K.: Static and dynamic stability of elastomeric bearings for seismic protection of structures. J. Struct. Eng. **139**, 1149–1159 (2013). https://doi.org/10.1061/(asce)st.1943-541x.0000660
52. Park, J.; Choun, Y.; Kim, M.: Effect of nonlinear hardening of lead rubber bearing on long term behavior of base isolated containment building. In: Trans. Korean Nucl. Soc. Spring Meetins, Jeju, Korea, pp. 7–8 (2015)
53. Ryan, K.L.; Kelly, J.M.; Chopra, A.K.: Nonlinear model for lead–rubber bearings including axial-load effects. J. Eng. Mech. **131**, 1270–1278 (2005). https://doi.org/10.1061/(ASCE)0733-9399(2005)131:12(1270)
54. Constantinou, M.C.; Whittaker, A.S.; Kalpakidis, Y.; Fenz, D.M.; Warn, G.P.: Performance of Seismic Isolation Hardware under Service Siesmic Loading, New York (2007)
55. Zelleke, D.H.; Elias, S.; Matsagar, V.A.; Jain, A.K.: Supplemental dampers in base-isolated buildings to mitigate large isolator displacement under earthquake excitations. Bull. New Zeal. Soc. Earthq. Eng (2015). https://doi.org/10.5459/bnzsee.48.2.100-117